Mesoscopic predictions of the effective thermal conductivity for microscale random porous media

Moran Wang,[1,*] Jinku Wang,[2] Ning Pan,[1] and Shiyi Chen[3]
[1]*Department of Biological & Agricultural Engineering, University of California, Davis, California 95616, USA*
[2]*School of Aerospace, Tsinghua University, Beijing 100084, China*
[3]*Department of Mechanical Engineering, Johns Hopkins University, Baltimore, Maryland 21218, USA*
(Received 13 July 2006; revised manuscript received 30 November 2006; published 7 March 2007)

A mesoscopic numerical tool has been developed in this study for predictions of the effective thermal conductivities for microscale random porous media. To solve the energy transport equation with complex multiphase porous geometries, a lattice Boltzmann algorithm has been introduced to tackle the conjugate heat transfer among different phases. With boundary conditions correctly chosen, the algorithm has been initially validated by comparison with theoretical solutions for simpler cases and with the existing experimental data. Furthermore, to reflect the stochastic phase distribution characteristics of most porous media, a random internal morphology and structure generation-growth method, termed the quartet structure generation set (QSGS), has been proposed based on the stochastic cluster growth theory for generating more realistic microstructures of porous media. Thus by using the present lattice Boltzmann algorithm along with the structure generating tool QSGS, we can predict the effective thermal conductivities of porous media with multiphase structure and stochastic complex geometries, without resorting to any empirical parameters determined case by case. The methodology has been applied in this contribution to several two- and three-phase systems, and the results agree well with published experimental data, thus demonstrating that the present method is rigorous, general, and robust. Besides conventional porous media, the present approach is applicable in dealing with other multiphase mixtures, alloys, and multicomponent composites as well.

DOI: 10.1103/PhysRevE.75.036702 PACS number(s): 02.70.Uu, 44.30.+v, 44.35.+c, 05.60.−k

I. INTRODUCTION

Transport phenomena in porous media have been investigated for over 100 years for applications in materials, agricultural, civil, and petroleum engineering [1,2]. Recently, more interests have been focused on heat and mass transfer processes in microporous media due mainly to their increasing importance in functional material design, fuel cell optimization, and even human biomedical engineering [3–6].

The effective thermal conductivity is one of the most important parameters characterizing the energy transport properties of porous media and has been studied extensively by using both theoretical and experimental approaches. As is well-known, the effective thermal conductivities of porous media depend not only on the thermal property and the volume fraction of each constitute component, but on the microstructures (i.e., the spatial distribution of all the components) of the media as well. The theoretical analyses of effective thermal conductivity found in the literature are generally based on the network combinations of the series and parallel models [7–11]. Carson *et al.* [12] and Wang *et al.* [13] have recently reviewed five fundamental models on effective thermal conductivity, including three dispersed-phase models developed according to the electric-magnetic theories [14,15]. Wang *et al.* [13] also presented some simple combinatory rules of these models in dealing with more complex materials. Almost all these theoretical models, however, ignore the often critical structural characteristics by assuming the multiphase materials as homogeneously dispersed systems. Also, the interactions among different components and phases are ignored in most cases. Therefore their predictions usually do not agree well with the experimental data.

Owing to the rapid developments of computers and computational techniques in the past few decades, numerical methods have been increasingly used to tackle the previously intractable mathematical equations so as to predict the effective thermal conductivities of real porous media [16–25]. For instance, Thovert *et al.* [16] calculated thermal conductivities of random media and regular fractals by solving the Laplace equation using the finite-difference method. Bakker [17] determined effective thermal properties of porous media through the finite element method. However, such numerical solvers for partial difference equations (PDE) encounter two challenges when the porous structures in question become complex [18,19]. The first is the constraint on the interphase conjugate heat transfer: for steady heat conduction through multiple phases, temperature and heat flux continuities have to be ensured at the interfaces. An extremely high computational resource is required in tackling this issue. Qian *et al.* [25] presented a two-dimensional five-speed (D2Q5) lattice Boltzmann model to calculate the effective thermal conductivity of porous media, while neglecting the solid-fluid conjugate heat transfer, which turned out to be a critical factor in such cases. The second challenge is the need of grid refinement for complex structures: the accuracy of a conventional numerical method is strongly dependent on the grid size and an extra fine grid is desired whenever the transport process is complex in physics and/or in geometry, and finer grid further drives the computational cost up often to an unrealistic level.

Another equally if not more difficult issue is to account for the influence of the usually complex structural geometry in a porous material system. Some stochastic-statistic methods representing the structural variations in porous media have gained attention recently [20,21]. For instance, Shos-

*Email address: mmwang@ucdavis.edu

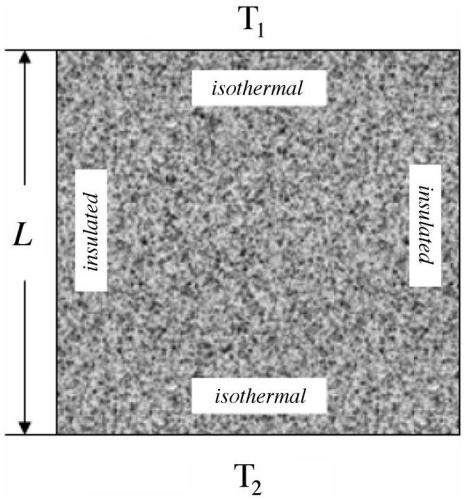

FIG. 1. Schematic diagram of domain and boundaries of heat transfer in porous media.

hany *et al.* [22] and Barta and Dieska [23] modeled the thermal conductivity of porous materials using the Monte Carlo method to reflect the structural fluctuations. Zhang *et al.* [24] in predicting the effective thermal conductivity of moist porous media developed a randomly mixed material model (RMM) to represent the structural influence, yielding results that agreed well with experimental data for porosity below 0.6.

The objective of this work is to develop a comprehensive approach for the more accurate prediction of the effective thermal conductivities of heterogeneous microporous media. To achieve this, we will first adopt a lattice Boltzmann method for multiphase conjugate heat transfer simulation in complex microstructures based on our previous work [26] by means of a spatially varying relaxation time. Next, we will devise a multiparameter tool based on the stochastic cluster growth theory to generate and control the random structures of complex porous media. After validation by some benchmarks, the present method will be applied to predict the effective thermal conductivities of various real microrandom porous media by comparing the modeling results with existing experimental data.

II. NUMERICAL METHODS

To determine the effective thermal conductivities of porous media, consider a two-dimensional pure conductive heat transfer problem in a system with both conducting phase and isolating phase, shown in Fig. 1, with negligible heat transfer caused by convection, radiation, and phase change. The contact thermal resistance between conducting phase is also small enough to neglect. The upper and lower boundaries are isothermal at T_1 and T_2, respectively. The left and right boundaries are insulated.

A. Governing equations

Therefore the energy equations for heat transfer in such a multiphase system, e.g., fluid and solid, without heat sources are

$$(\rho c_p)_f \left(\frac{\partial T}{\partial t} \right) = k_f \nabla^2 T, \tag{1}$$

$$(\rho c_p)_s \left(\frac{\partial T}{\partial t} \right) = k_s \nabla^2 T, \tag{2}$$

where subscript f represents the fluid, and s the solid; T is the temperature, ρ the density, k the thermal conductivity, and c_p the specific heat capacity.

At the interfaces between the two phases once in equilibrium, the temperature and heat flux continuities have to be satisfied with no contact thermal resistance at the interfaces,

$$T_{f,\text{int}} = T_{s,\text{int}}, \tag{3}$$

$$k_f \left. \frac{\partial T}{\partial \hat{n}} \right|_{f,\text{int}} = k_s \left. \frac{\partial T}{\partial \hat{n}} \right|_{s,\text{int}}, \tag{4}$$

where the subscript "int" corresponds to the interfaces and $\hat{n}$ represents the unit normal vector to the interfaces. Equations (1)–(4) describe a classical case of the multiphase conjugate heat transfer problem [24,27]. As stated above, this constraint of continuity at an interface increases the computational costs tremendously when using the conventional numerical methods. Moreover, since there are huge numbers of such interfaces in porous media, this further pushes the computational expense into prohibition. We thus have to adopt another route as introduced in the next section.

Once the temperature field is derived, the effective thermal conductivity, k_{eff}, can be determined as

$$k_{\text{eff}} = qL/\Delta T, \tag{5}$$

where q is the steady heat flux through the media between the temperature difference ΔT over a thickness L.

B. Lattice Boltzmann algorithm

The lattice Boltzmann method (LBM) is intrinsically a mesoscopic approach based on the evolution of statistical distribution of lattices, and has achieved considerable success in simulating fluid flows and associated transport phenomena [28–30]. The most important advantages of LBM are the easy implementation of multiple interparticle interactions and complex geometry boundary conditions [31,32]. Conservations can generally hold automatically without additional computational efforts [33,34]. Models specifically on thermal behaviors based on the LBM have been developed recently [35]. Here we further develop our previous work on the lattice Boltzmann algorithm for the fluid-solid conjugate heat transfer problem [26].

For pure thermal conduction in porous media governed by Eqs. (1) and (2), the evolution equation for a two-dimensional nine-speed (D2Q9) LBM in both liquid and solid phases can be generally given as [26,35]

$$g_\alpha(\mathbf{r} + \mathbf{e}_\alpha \delta_t, t + \delta_t) - g_\alpha(\mathbf{r}, t) = -\frac{1}{\tau}[g_\alpha(\mathbf{r}, t) - g_\alpha^{\text{eq}}(\mathbf{r}, t)], \tag{6}$$

where $\mathbf{r}$ is the location vector, t the real time, δ_t the time step, g^{eq} the equilibrium distribution of the evolution variable g_α

$$g_\alpha^{\mathrm{eq}} = \begin{cases} 0, & \alpha = 0 \\ \frac{1}{6}T, & \alpha = 1-4 \\ \frac{1}{12}T, & \alpha = 5-8, \end{cases} \tag{7}$$

$\mathbf{e}_\alpha$ is the discrete velocity

$$\mathbf{e}_\alpha = \begin{cases} (0,0), & \alpha = 0 \\ (\cos\theta_\alpha, \sin\theta_\alpha)c, \theta_\alpha = (\alpha-1)\pi/2, & \alpha = 1-4 \\ \sqrt{2}(\cos\theta_\alpha, \sin\theta_\alpha)c, \theta_\alpha = (\alpha-5)\pi/2 + \pi/4, & \alpha = 5-8 \end{cases} \tag{8}$$

and τ the dimensionless relaxation time for each phase which is determined by the corresponding thermal conductivity,

$$\tau_s = \frac{3}{2}\frac{k_s}{(\rho c_p)_s c^2 \delta_t} + 0.5, \tag{9}$$

and

$$\tau_f = \frac{3}{2}\frac{k_f}{(\rho c_p)_f c^2 \delta_t} + 0.5. \tag{10}$$

c is a *pseudo* sound speed, defined as δ_x/δ_t, where δ_x is the lattice constant (i.e., the grid size), whose value in theory can take any positive number just to insure τ to be within (0.5, 2) [26,30]. A larger c may result in a more accurate temperature prediction near the boundaries, yet with higher computational costs [26]. Not to violate the requirement of temperature and heat flux continuities at phase interfaces, we have to assume identical volume thermal capacities (ρc_p) for different phases; the conjugate heat problem between different phases is thus solved and these assumptions will not affect the effective thermal conductivity calculated [36]. The temperature and the heat flux can then be calculated as [37]

$$T = \sum_\alpha g_\alpha, \tag{11}$$

$$q = \left(\sum_\alpha c_\alpha g_\alpha\right)\frac{\tau - 0.5}{\tau}. \tag{12}$$

C. Boundary conditions

For the isothermal boundary treatment, we follow the bounce-back rule of the nonequilibrium distribution proposed by Zou and He [38]

$$g_\alpha - g_\alpha^{\mathrm{eq}} = -(g_\beta - g_\beta^{\mathrm{eq}}), \tag{13}$$

where the subscripts α and β represent the opposite directions, and the equilibrium distribution can be calculated using the local boundary temperatures.

For the insulated boundary, we use the Neumann boundary treatment [26,37] and let the boundary temperature gradient equal to zero. However, heat flux leak will result along the insulated surfaces. Therefore a special reflection boundary condition is implemented here,

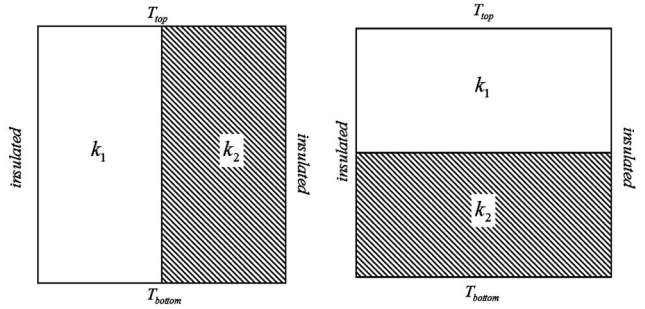

FIG. 2. Two basic structures for validation. (a) Parallel mode and (b) series mode.

$$g_\alpha = g_\beta. \tag{14}$$

These boundary treatments have approximately a second order accuracy [38].

III. BENCHMARKS

To validate the present method, we first compare the predicted results with existing simpler theoretical solutions and also some experimental data of real material structures.

A. Existing theoretical solutions

First we calculate the effective thermal conductivities for two basic structures of dual-component materials: the parallel mode and the series mode (see Fig. 2). Assuming the thermal conductivity of each component is k_1 and k_2, respectively, the simple theoretical solutions offer the effective thermal conductivities as $(k_1+k_2)/2$ for the parallel mode and $1/(1/2k_1+1/2k_2)$ for the series mode.

Table I lists the calculated effective thermal conductivities compared with theoretical solutions for different values of $k_1:k_2$. We keep k_1 as 1.0 W/m K while changing k_2 from 2.0 to 10 000 W/m K. Such a large contrast between k_1 and k_2 leads to a long computational time for our algorithms to converge to a steady result, and yet provides a good test of our model. The deviations between the predictions are no greater than 0.006% for the parallel mode and 0.765% for the series mode even for very large conductivity contrasts, showing good accuracy of our approach.

B. Experimental data

Figure 3 shows the two-dimensional (2D) pore structure profiles truncated at two perpendicular cross directions of a three-dimensional heterogeneous polyurethane foam [39]. In each figure, the white part is the solid polyurethane and the dark part is the air. Measured data for the material are made available from Ref. [39]. These structures were scanned and transferred to 200×200 data matrices and then used for simulations in [40]. We calculate the effective thermal conductivities for the two given structures using our present method and compare them with the measured data from Ref. [39]. The results listed in Table II show that the deviations of

TABLE I. Comparisons between predicted results and theoretical solutions, where $k_1=1.0$ (W/m K).

	Results					
	Parallel mode			Series mode		
$k_1:k_2$	Theoretical value (W/m K)	Present predictions (W/m K)	Relative deviations (%)	Theoretical value (W/m K)	Present predictions (W/m K)	Relative deviations (%)
1:2	1.500	1.500	0.000	1.333	1.332	0.075
1:10	5.500	5.500	0.000	1.818	1.815	0.165
1:100	50.50	50.50	0.000	1.980	1.976	0.202
1:500	250.5	250.5	0.000	1.996	1.991	0.250
1:1000	500.5	500.5	0.000	1.998	1.993	0.250
1:10000	5000.5	5000.2	0.006	1.9998	2.0151	0.765

the predicted effective thermal conductivities are no greater than 15.0%. It is expected that more finely scanned structure profiles and improved experimental measurements would lead to closer agreements.

IV. RANDOM POROUS MEDIA GENERATION: THE QSGS TOOL

Generally, it is extremely difficult if not impossible to completely describe the microstructure of a porous medium due to its complex and stochastic nature. One can only acquire some statistic-based average information such as the mean porosity or better, the pore size distribution. This problem has to be solved if the full details of a porous structure need to be brought into formulation for more rigorous treatment. In fact, more accurate predictions of transport characteristics of porous media require more detailed descriptions of the entire porous media morphology, including both the geometric properties such as grain or pore shape, and the volumetric and topological properties such as pore tortuosity and interconnectivity. Several such attempts have been reported. The reconstruction process is a popular method to reproduce porous structures [41]; however, determinations of the correlation functions are very complicated. The random location of obstacles is the simplest one to construct an artificial porous medium when other microstructure details are negligible [22–24]. To adjust the pores size and connectivity, Coveney *et al.* [42] proposed a pore growth-with-time model. By developing this idea from [42] further in connection with the cluster growth theories in [43], we propose in this paper a more comprehensive approach in which four parameters are identified for controlling the internal porous structure of granular media, thus forming a set termed the quartet structure generation set (QSGS). This set enables us to generate porous morphological features closely resembling the forming progress of many real porous media.

A. Algorithm description

The flowchart of the QSGS process is shown in Fig. 4 and the algorithm is described as follows. Before initiation, one has to determine among the different phases in a system a nongrowing phase and the rest are growing ones. For generality, we call the growing phase the nth phase, where $n=2$ to N, the total number of phases in the system. Customarily without losing generality, the discrete phases are normally taken as the growing phases. For example, rocks and moisture are the growing phases in unsaturated sands, whereas gas is the growing phase in polyurethane foams. Then the growing process follows the steps below.

(i) Randomly locate the cores of the first growing phase in a grid system based on a core distribution probability, c_d, whose value is no greater than the volume fraction of the phase. Each cell in the grid will be assigned a random number by a uniform distribution function within (0, 1). Each cell whose random number is no greater than c_d will be chosen as a core.

(ii) Enlarge every element of the growing phase to its neighboring cells in all directions based on each given directional growth probability, D_i, where i represents the direction. Again for each growing element, new random numbers

TABLE II. Comparisons between present predictions and experimental data for given structures, where $k_s=0.58$ (W/m K), $k_g=0.0083$ (W/m K), and the subscripts s and g as in the original paper represent solid and gas, respectively.

Along the foam growing direction			Across the foam growing direction		
Prediction (W/m K)	Experiment (W/m K)	Deviation (%)	Prediction (W/m K)	Experiment (W/m K)	Deviation (%)
0.0253	0.0220	15.0	0.0265	0.0245	8.16

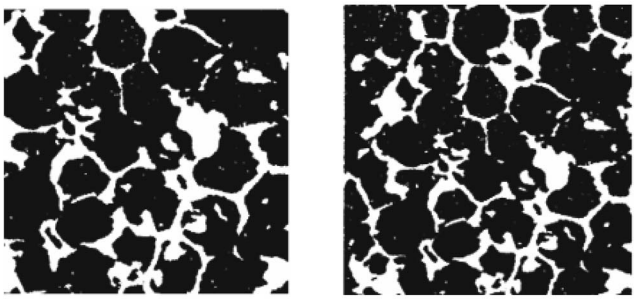

(a) Along the foam growing direction (b) Cross the foam growing direction

FIG. 3. Given structures of the polyurethane foam [39]. (a) Along the foam growing direction and (b) Across the foam growing direction.

will be assigned to its neighboring cells. The neighboring cell in direction i will become part of the growing phase if its random number is no greater than D_i.

(iii) Repeat the growing process of (ii) until the volume fraction of the first growing phase reaches its given value P^2 (if the growing phase is gas, P^2 is more often expressed as the porosity ε).

(iv) As to the next growing phase, there are two cases to consider depending on its interaction with the existing phase(s). If this phase is an equivalent discrete phase as the existing growing phase, such as multicomponent mixture, it grows from separate seeds, which is very similar as the first growing phase described in (i)–(iii). Otherwise, we have to consider the constraint by and interaction with the existing phase(s). For such cases, the nth phase ($n>2$) will grow based on a phase interaction growth probability, $I_i^{n,m}$, which represents the growth probability of the nth phase on the mth phase along the ith direction.

(v)Stop the nth phase growth once its volume fraction reaches the given value P^n.

(vi) Repeat the next phase growth as described in (iv) and (v) until n=N.

(vii) The spaces not occupied at the end represent the nongrowing phase.

B. More on the growth parameters

Since the four parameters (c_d, D_i,P^n, and $I_i^{n,m}$) essentially control the microstructure characteristics of the generated porous media based on our QSGS process, we discuss here in detail the effects of their values on the morphology features.

The core distribution probability c_d is defined as the probability of a cell to become a core of the first growing phase on which growth or expansion of the first phase originates. The value of c_d indicates the number density of growing cores for the first growing phase, to reflect the statistical distribution of the first growing phase throughout the system. For example, if we know from experimental data that there are 40 particles of a solid phase *in statistics* in a focused system and we want to reproduce such a structure on a 200 $\times$200 grid, the value of c_d for this phase (if chosen as the first growing phase) 40/40 000=0.001, meaning every cell

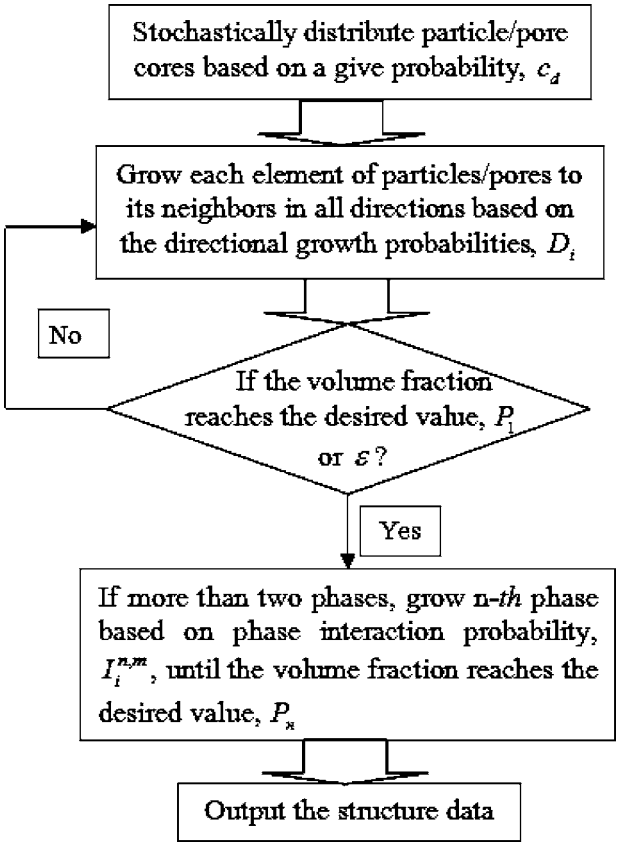

FIG. 4. Flowchart of the QSGS process.

in the grid has a probability of 0.001 to be a core of that solid phase. The value of c_d thus also controls the degree of structure details of a system; a smaller c_d leads to a finer description of the microstructures including particle-pore shapes and interparticle-pore connections. However, a small value of c_d will decrease the statistical particle numbers under a given grid number and thus increase the computation fluctuation.

The directional growth probability D_i is defined as the probability for an unoccupied cell to expand into a neighboring cell in the ith direction so as to become part of the first growing phase. An appropriate arrangement of the directional growth probabilities may lead to an isotropic structure of porous media. In other words, the growth probabilities can

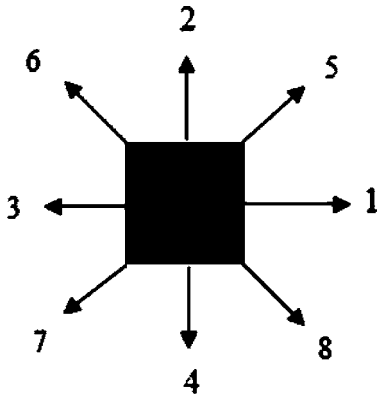

FIG. 5. Eight growth directions of each point in 2D systems.

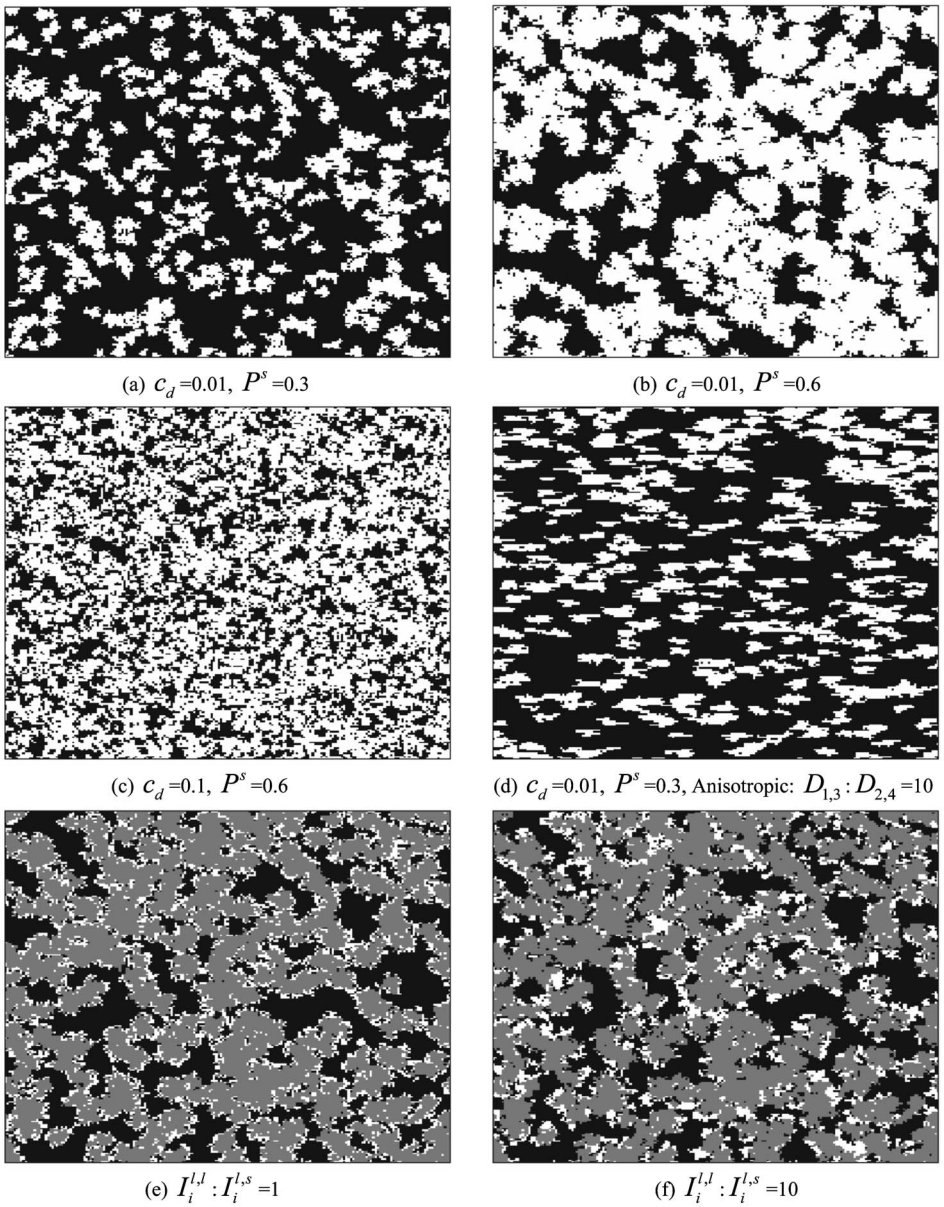

FIG. 6. Schematics of the generated porous media using the present method (200×200).

be adjusted to control the degree of anisotropy. For two-dimensional cases, each square elemental cell has eight growing directions to its neighbors, see Fig. 5. There are four main directions (1,2,3,4) and four diagonal directions (5,6,7,8). For simplicity, we abbreviate the four directional growth probabilities D_1, D_2, D_3, and D_4, for example, into $D_{1,2,3,4}$ or even D_{1-4} when appropriate. To obtain an isotropic structure in such systems, we have to set uniform main directional growth probabilities D_{1-4} and uniform diagonal directional growth probabilities D_{5-8}, respectively. By setting the probabilities ratio, $D_{1-4}:D_{5-8}=4$, we make the directional growth probability consistent with the equilibrium density distribution function for isotropic materials [44]. This assumption needs more rigorous validation in the future; yet it works well in our simulations. It is the relative value not the absolute value of D_i that controls the anisotropy of the structure. Since the growing process is a repeating loop, a smaller value of D_i will lead to a more accurate reaching of the desired volume fraction of the growing phase with higher computational costs. In most of our practices, we use 0.0001 for the diagonal directional growth probabilities.

For multiphase porous media systems ($N\geqslant3$) if there are phase interactions between different discrete phases, we have to consider the effects of phase interactions on the phase distributions during the successive phase growth. Such effects are important especially, for instance, in unsaturated porous media soaked by a liquid that wets other phases in the system differently. In such systems, the growth order of the growing phases is important. Generally the solid phase is selected as the first growing phase and the liquid phase grows under the effects of phase interactions. The phase interaction growth probability, $I_i^{n,m}$, i.e., the growth probability of the nth phase on the surface of the mth phase along the ith direction, is hence introduced to account for this influence by assigning different values to $I_i^{n,m}$ for different materials. For example, in a sands-liquid-air system, the sands and liquid

are the first and the second growing phase, respectively. The bonding of liquid onto the sands surfaces depends on the wetting property of the sands. If the wetting property of the sands is hydrophilic, the liquid will be readily covering the sands surfaces. That means the liquid-solid affinity is greater than that of liquid-liquid and the liquid phase should combine more easily to the solid phase than to the liquid phase so that $I_i^{3,3} < I_i^{3,2}$ or the ratio $I_i^{3,3}:I_i^{3,2}$ should be no greater than 1, where the superscript 3 represents the liquid and 2 the solid. The value of the phase interaction growth probability $I_i^{n,m}$ could be determined by analyzing the scanned pictures of the phase distributions or by calculating from the wetting properties directly.

Figure 6 shows six schematic illustrations of the generated porous structures using the present QSGS method. The stochastic characteristics are depicted rather realistically in the figures. The first four figures are two-phase cases, where the white area represents the growing phase (solid) and the black the nongrowing phase (gas). The parameters for Fig. 6(a) are $c_d=0.01$, $P^s=0.3$, and $D_{1,3}=D_{2,4}=4D_{5-8}$. Figure 6(b) shows the case where the solid volume fraction P^s geminates where both the volume and the interparticle connections of the solid phase increase. Comparison between Figs. 6(b) and 6(c) shows the effect of the core distribution probability c_d on the generated microstructure. A higher value of c_d leads to a more uniform phase distribution of medium. When the directional growth probability is changed in some direction, the isotropy will be destroyed. Figure 6(d) shows the generated anisotropic structure where the horizontal growth probability is ten times the vertical one, $D_{1,3}=10D_{2,4}$ and $D_{2,4}=4D_{5-8}$. Figures 6(e) and 6(f) show phase distributions of three-phase porous media by different phase interaction probabilities. The black is the nongrowing phase (gas), the gray is the first growing phase (solid), and the white is the second growing phase (liquid). The phase interaction probability changes the distribution status of the second growing phase. A high value of liquid-solid interaction means a strong wetting property of the liquid on the solid surface. The liquid will distribute like a film on the solid surface as shown in Fig. 6(e). On the contrary, a strong liquid-liquid interaction probability leads to a high degree of liquid conglomeration. The liquid exists as droplets or liquid-bridges on the solid particles [see Fig. 6(f)]. The effects of phase distribution on the effective properties of porous media will be investigated in detail in our future work.

C. Uncertainty analysis

Since the random fluctuations have been introduced during the generation of porous structures, the calculated effective thermal conductivity for a given porous medium with statistical characteristics in its structure will not be identical in every trial, but fluctuates around an average value. The scope of the fluctuations mainly depends on the grid size (cell numbers) and the particle numbers (sample size). A larger grid size and/or greater particle number will improve the simulation accuracy, yet will increase the computational costs as well. Our tests have demonstrated that the variations caused by such systematic fluctuation are no greater than 3% for two-dimensional two-phase cases with a 200×200 grid and $c_d=0.01$ [45].

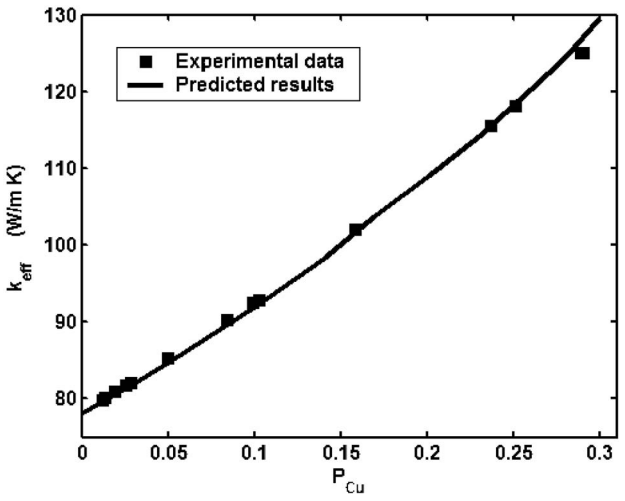

FIG. 7. Comparisons between predictions and experimental data for Cu/solder material. The experimental data is from Ref. [46]. The parameters are $k_{Cu}=398.0$ W/m K and $k_{solder}=78.1$ W/m K.

V. RESULTS AND DISCUSSION

Next the effective thermal conductivities for different types of porous materials are predicted using the present mesoscopic numerical method, consisting of the lattice Boltzmann solver in combination with the QSGS tool. Both two-phase and three-phase cases are considered and the numerical predictions are then compared with the existing experimental data from the literature for the same cases. Since in the literature no structure details have been reported together with the measured effective thermal conductivities, we can only use estimated values for the QSGS parameters in the following simulations. Unless specified otherwise, we set the parameters in the QSGS tool as follows: $c_d=0.01$ and $D_{1-4}=4D_{5-8}$ for two-phase materials and $I_i^{3,2}=I_i^{3,3}$ for three-phase porous media. Thus the only required input variables are the thermal conductivity and the relative volume fraction for each component or phase.

A. Two-phase cases

First we consider a two-solid phase composite, Cu/solder where the Cu particles are dispersed inside the solder mass [46]. The component thermal conductivities are $k_{Cu}=398.0$ W/m K and $k_{solder}=78.1$ W/m K, respectively. Figure 7 shows the predicted effective thermal conductivities as a function of the volume fraction of Cu, compared with the experimental data from [46]. Good agreement is shown.

The present method can also be used to predict the effective thermal conductivity of two-phase suspension. Here we consider a graphite/water suspension where the volume fraction of graphite is $P^{Graphite}$, dispersed into water to form an aqueous solution. The thermal conductivities of graphite and water are $k_{Graphite}=160.5$ W/m K and $k_{water}=0.666$ W/m K, respectively. The predicted effective thermal conductivities

TABLE III. Effective thermal conductivities of graphite/water suspension.

		Jagjiwanram's predictions		Present predictions	
P_{Graphite}	k_{eff} (expt.) (W/m K)	k_{eff} (W/m K)	Deviation (%)	k_{eff} (W/m K)	Deviation (%)
0.05	0.832	0.862	3.61	0.800	−3.85
0.11	1.132	1.004	−11.31	1.004	−11.31
0.17	1.439	1.145	−20.43	1.286	−10.63

are compared in Table III with both the experimental data and the predicted values using Jagjiwanram's resistor model [47]. All results are in relatively good agreement. Note that our predictions are always lower than the measured data; likely because the present model does not consider the movement of the suspended phase which could be an important factor in enhancing the heat transfer in suspensions [48].

B. Three-phase cases

Unsaturated porous media are studied in this section as well where there are three phases in the system. Customarily, the porosity, ε, is defined as the total volume fraction of the fluids. The degree of saturation, S, is defined as the liquid volume fraction within the fluids. Therefore the solid phase, the liquid phase, and the gas phase have the volume fractions of $(1-\varepsilon)$, εS, and $\varepsilon(1-S)$, respectively. In the present work, we assume the liquid phase is uniformly attached onto the solid surfaces, which means $I_i^{3,2}=I_i^{3,3}$ in each direction i.

Figure 8 shows the predicted effective thermal conductivities versus the degree of saturation S for moist porous brick sands under both frozen and unfrozen states. The numerical results are compared again with the experimental data from [49,50]. The simulation parameters include $\varepsilon=0.52$, $k_s=2.85$ W/m K, $k_w=0.5924$ W/m K, $k_g=0.0249$ W/m K, and $k_{\text{ice}}=2.38$ W/m K [50,51]. A 200×200 grid is used in the simulations, yielding the random fluctuation within 3%. Once again, good agreements are obtained for both frozen and unfrozen cases [52].

The predictions for another three-phase case, wetting glass particle assemblies, are also compared with the recent experimental data by Kohout *et al.* [53]. The simulation parameters are $\varepsilon=0.39$, $k_s=0.8$ W/m K, $k_w=0.61$ W/m K, and $k_g=0.025$ W/m K. Figure 9 illustrates the predicted results along with the experimental data, as well as with other theoretical modeling results from Ref. [53]. A better consistence between the present predictions with the experiments is again exhibited.

VI. CONCLUSIONS

A mesoscopic numerical model for predicting the effective thermal conductivity of multiphase microporous media has been established in this paper. The model is a combination of two parts. A random generation-growth method, named quartet structure generation set (QSGS), was first proposed based on the stochastic cluster growth theory for gen-

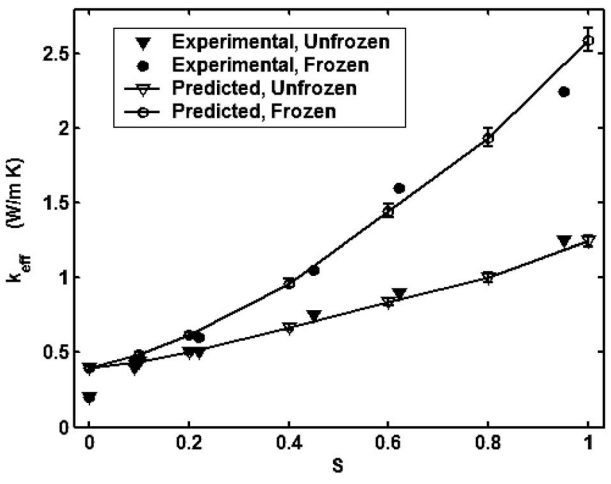

FIG. 8. Comparisons between predicted and experimental effective thermal conductivities of unsaturated porous sands in frozen and unfrozen states. The experimental data is from Refs. [49,50]. The parameters are $\varepsilon=0.52$, $k_s=2.85$ W/m K, $k_w=0.5924$ W/m K, $k_g=0.0249$ W/m K, and $k_{\text{ice}}=2.38$ W/m K.

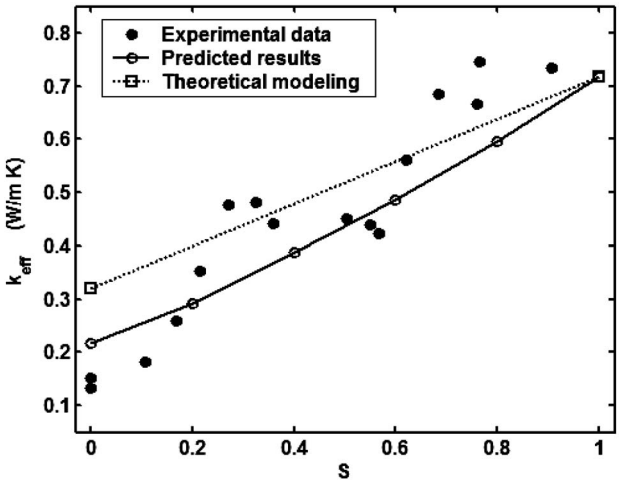

FIG. 9. The effective thermal conductivity vs degree of saturation of wetting glass assemblies. The experimental data and the theoretical solutions are from Ref. [53]. The simulation parameters are $\varepsilon=0.39$, $k_s=0.8$ W/m K, $k_w=0.61$ W/m K, and $k_g=0.025$ W/m K.

erating various microstructures of multiphase porous media. A lattice Boltzmann algorithm considering multiphase conjugate heat transfer was then developed to tackle the thermal conduction phenomena in the multiphase porous media with second-order accurate boundary treatments. After benchmark validations, the present model has then been applied to predict the effective thermal conductivity for both two-phase and three-phase porous materials successively, and the numerical predictions agreed well with the published experimental data in each case. The present method is not limited to the conventional porous media, but is also suitable for most if not any multiphase mixtures or multicomponent composites. With no empirical parameters to be determined case by case, this method is highly promising as a realistic, reliable, and robust tool dealing with various complex thermal transport problems in porous media and mixed multiphase systems.

ACKNOWLEDGMENTS

The authors would like to thank Dr. Shi, Mingheng for providing us the structure data of the polyurethane foam and Dr. Stepanek for providing us the experimental data. The authors would also like to thank the helpful discussions from Dr. Zhang, Haifeng, and Dr. Carson, James K.

[1] M. Muskat, *The Flow Of Homogeneous Fluids Through Porous Media* (McGraw-Hill, New York, 1937).
[2] R. W. Zimmerman, *Compressibility of Sandstones* (Elsevier, New York, 1991).
[3] D. B. Ingham, A. Bejan, E. Mamut, and I. Pop, *Emerging Technologies and Techniques in Porous Media* (Kluwer, London, 2003).
[4] A. Sayari and M. Jaroniec, *Nanoporous Materials IV* (Elsevier, New York, 2005).
[5] D. B. Ingham and I Pop, *Transport Phenomena in Porous Media III* (Elsevier, Oxford, UK, 2005).
[6] N. Pan and W. Zhong, *Fluid Transport Phenomena in Fibrous Materials* (Woodhead, Cambridge, UK, 2006).
[7] A. Bouguera, J. Phys. D **32**, 2797 (1999); **32**, 1407 (1999).
[8] X. G. Liang and W. Qu, Int. J. Thermophys. **42**, 1885 (1999).
[9] J. E. J. Staggs, Fire Saf. J. **37**, 107 (2002).
[10] R. Singhand and H. S. Kasana, Appl. Therm. Eng. **24**, 1841 (2004).
[11] Y. T. Ma, B. M. Yu, D. M. Zhang, and M. Q. Zou, J. Appl. Phys. **95**, 6426 (2004).
[12] J. K. Carson, S. J. Lovatt, D. J. Tanner, and A. C. Cleland, J. Food. Eng. **75**, 297 (2006).
[13] J. F. Wang, J. K. Carson, M. F. North, and D. J. Cleland, Int. J. Heat Mass Transfer **49**, 3075 (2006).
[14] J. C. Maxwell, *A Treatise on Electricity and Magnetism* 3rd ed. (Dover, New York 1954).
[15] M. Christon, P. J. Burns, and R. A. Sommerfeld, Numer. Heat Transfer, Part A **25**, 259 (1994); G. Buonanno and A. Carotenuto, *ibid.* **37**, 343 (2000); R. P. A. Rocha and M. E. Cruz, *ibid.* **39**, 179 (2001).
[16] J. F. Thovert, F. Wary, and P. M. Adler, J. Appl. Phys. **68**, 3872 (1990); D. Coelho, J. F. Thovert, and P. M. Adler, Phys. Rev. E **55**, 1959 (1997).
[17] K. Bakker, Int. J. Heat Mass Transfer **40**, 3503 (1997).
[18] A. G. Fedorov and R. Viskanta, Int. J. Heat Mass Transfer **43**, 399 (2000); A. Horvat and I. Catton, *ibid.* **46**, 2155 (2003).
[19] G. S. Springer and S. W. Tsai, J. Compos. Mater. **1**, 166 (1967); R. Pal, *ibid.* **39**, 1147 (2005).
[20] D. X. Zhang, *Stochastic Method for Flow in Porous Media* (Academic Press, London, 2002).
[21] D. Kulasiri and W. Verwoerd, *Stochastic Dynamics Modeling Solute Transport in Porous Media* (Elsevier, New York, 2002).
[22] Y. Shoshany, D. Prialnik, and M. Podolak, Icarus **157**, 219 (2002).
[23] S. Barta and P. Dieska, Kovove Mater. **40**, 99 (2002).
[24] H. F. Zhang, X. S. Ge, and H. Ye, Modell. Simul. Mater. Sci. Eng. **13**, 401 (2005); H. F. Zhang, X. S. Ge, and H. Ye, J. Phys. D **39**, 220 (2006).
[25] J. Y. Qian, Q. Li, K. Yu, and Y. M. Xuan, Sci. China, Ser. E: Technol. Sci. **47**, 716 (2004).
[26] J. K. Wang, M. Wang, and Z. X. Li, Int. J. Therm. Sci. **46**, 228 (2007).
[27] D. B. Ingham and I. Pop, *Transport Phenomena in Porous Media III* (Elsevier, San Diego, 2005).
[28] S. Y. Chen and G. D. Doolen, Annu. Rev. Fluid Mech. **30**, 329 (1998).
[29] D. Raabe, Modell. Simul. Mater. Sci. Eng. **12**, R13 (2004).
[30] J. K. Wang, M. Wang, and Z. X. Li, J. Colloid Interface Sci. **296**, 729 (2006); M. Wang, J. K. Wang, and Z. X. Li, *ibid.* **300**, 446 (2006).
[31] Q. J. Kang, D. X. Zhang, and S. Y. Chen, J. Geophys. Res., [Solid Earth] **108**, 2505 (2003); Q. J. Kang, D. X. Zhang, P. C. Lichtner, and I. N. Tsimpanogiannis, Geophys. Res. Lett. **31**, L21604 (2004).
[32] M. Wang, J. K. Wang, S. Y. Chen, and N. Pan, J. Colloid Interface Sci. **304**, 246 (2006).
[33] G. D. Doolen, *Lattice Gas Methods for Partial Differential Equations* (Addison-Wesley, New York, (1990).
[34] S. Succi, *The Lattice Boltzmann Equation for Fluid Dynamics and Beyond* (Oxford Science Press, London 2001).
[35] X. Y. He, S. Y. Chen, and G. D. Doolen, J. Comput. Phys. **146**, 282 (1998); Y. Peng, C. Shu, and Y. T. Chew, Phys. Rev. E **68**, 026701 (2003).
[36] X. Chen and P. Han, Int. J. Heat Fluid Flow **21**, 463 (2000).
[37] A. D'Orazio and S. Succi, Lect. Notes Comput. Sci. **2657**, 977 (2003).
[38] Q. S. Zou and X. Y. He, Phys. Fluids **9**, 1591 (1997).
[39] M. H. Shi and X. K. Zong, J. Southeast Univ. **6**, 76 (1990).
[40] X. C. Li, M. H. Shi, and D. H. Zhang, in *The 11th National Academic Conference on Engineering Thermophysics of China. Shanghai, China* (2002) pp. 512.
[41] S. Torquato, *Random Heterogeneous Materials: Microstructure and Macroscopic Properties* (Springer, New York, 2002); I. M. Young, J. W. Crawford, and C. Rappoldt, Soil Tillage

Res. **61**, 33 (2001).
[42] P. V. Coveney, J. B. Maillet, J. L. Wilson, P. W. Fowler, O. Al-Mushadani, and B. M. Boghosian, Int. J. Mod. Phys. C **9**, 1479 (1998).
[43] P. Meakin, *Fractals, Scaling and Growth Far From Equilibrium* (Cambridge University Press, Cambridge, England, 1998).
[44] X. He and L. S. Luo, Phys. Rev. E **55**, R6333 (1997); T. Abe, J. Comput. Phys. **131**, 241 (1997).
[45] The uncertainty results mainly from the generated random structure of porous media. The fluctuation of the predictions depends on the sample size, which is mostly relative to the pore number. For a finite computational resource, one has to find a balance between the transport details and the statistical errors.
[46] H. J. Lee and R. E. Taylor, J. Appl. Phys. **47**, 148 (1976).
[47] Jagjiwanram and R. Singh, Bull. Mater. Sci. **27**, 373 (2004).
[48] R. Prasher, P. Bhattacharya, and P. E. Phelan, Phys. Rev. Lett. **94**, 025901 (2005).
[49] A. R. Sepaskhah and L. Boersma, Soil Sci. Soc. Am. J. **43**, 439 (1979).
[50] A. K. Singh, R. Singh, and D. R. Chaudhary, **23**, 698 (1990).
[51] S. Fukusako, Int. J. Thermophys. **11**, 353 (1990).
[52] Because the effective thermal conductivity of a mixture must not be higher than the highest thermal conductivity among all the components, we deduce that the experimental value for the frozen case at $S \approx 0.95$ is overrated in Fig. 2 of Ref. [51]. The succedent Fig. 5 in the same article proved this point. Therefore the experimental data is modified by comparing Figs. 2 and 5 in Ref. [51].
[53] M. Kohout, A. P. Collier, and F. Stepanek, Int. J. Heat Mass Transfer **47**, 5565 (2004).